Light charged Higgs boson scenario in 3-Higgs doublet models

A. G. Akeroyd,[1, *] Stefano Moretti,[1, †] Kei Yagyu[1, ‡] and Emine Yildirim[1, §]

[1]*School of Physics and Astronomy, University of Southampton,*

Southampton, SO17 1BJ, United Kingdom

Abstract

The constraints from the measurements of the $B \to X_s \gamma$ decay rate on the parameter space of 3-Higgs Doublet Models (3HDMs), where all the doublets have non-zero vacuum expectation values, are studied at the next-to-leading order in QCD. In order to naturally avoid the presence of flavour changing neutral currents at the tree level, we impose two softly-broken discrete Z_2 symmetries. This gives rise to five independent types of 3HDMs that differ in their Yukawa couplings. We show that in all these 3HDMs (including the case of type-II-like Yukawa interactions) both masses of the two charged Higgs bosons $m_{H_1^\pm}$ and $m_{H_2^\pm}$ can be smaller than the top mass m_t while complying with the constraints from $B \to X_s \gamma$. As an interesting phenomenological consequence, the branching ratios of the charged Higgs bosons decay into the cb final states can be as large as 80% when their masses are taken to be below m_t in two of the five 3HDMs (named as Type-Y and Type-Z). This light charged Higgs boson scenario provides a hallmark 3HDM signature that cannot be realised in Z_2 symmetric 2-Higgs doublet models. We find that in the Type-Y and Type-Z 3HDMs the scenario with $90 \, \text{GeV} < m_{H_1^\pm}, m_{H_2^\pm} < m_t$ is ruled out by the direct searches at the LHC, but in the Type-Y 3HDM $80 \, \text{GeV} < m_{H_1^\pm} < 90 \, \text{GeV}$ and $90 \, \text{GeV} < m_{H_2^\pm} < m_t$ is allowed by $B \to X_s \gamma$ and direct searches at LEP2, Tevatron and LHC due to the reduced sensitivity of these searches to the degenerate case $m_{H_1^\pm} \approx m_{W^\pm}$. The cases where only one or both charged Higgs bosons are above the top quark mass are also naturally allowed in the both Type-Y and Type-Z 3HDMs.

*Electronic address: A.G.Akeroyd@soton.ac.uk

†Electronic address: S.Moretti@soton.ac.uk

‡Electronic address: K.Yagyu@soton.ac.uk

§Electronic address: ey1g13@soton.ac.uk

arXiv:1605.05881v2 [hep-ph] 14 Feb 2017

I. INTRODUCTION

After the 7 and 8 TeV runs of the CERN Large Hadron Collider (LHC), it has been clarified that a Higgs boson exists with a mass of about 125 GeV and that its measured properties – such as the signal strengths of various production and decay channels – are consistent with those of the Standard Model (SM) Higgs boson [1, 2]. Although this suggests the existence of an isospin doublet scalar field, there remains an open question: i.e., how many doublets are there in the actual Higgs sector?

The existence of a second Higgs doublet is strongly expected when we consider physics Beyond the SM (BSM). The most familiar example is the case of supersymmetric extensions of the SM, in which at least two Higgs doublets are required to generate all the masses of charged fermions and for anomaly cancellation [3]. In addition, extra sources of CP-violation can be obtained from Higgs sectors with a multi-doublet structure, an ingredient which is necessary to realise a successful scenario based on Electro-Weak (EW) baryogenesis [4–6]. Furthermore, the second doublet is often introduced in models for neutrino masses [7] and dark matter [8]. Therefore, adopting a bottom-up approach while studying the phenomenology of multi-Higgs-doublet models is important in order to access BSM physics.

One of the characteristic features of extended Higgs models is the appearance of charged Higgs bosons, so that their detection can be taken as direct evidence of such structures. In particular in multi-doublet models, singly charged Higgs bosons can affect various flavour observables such as B-meson related processes. For example, $B \to X_s\gamma$ data give a lower limit on the mass and Yukawa couplings of charged Higgs bosons. In Refs. [9–12], the Branching Ratio (BR) of $B \to X_s\gamma$ has been calculated at the Next-to-Leading Order (NLO) in QCD in the context of 2-Higgs Doublet Models (2HDMs) with a softly-broken Z_2 symmetry. In Refs. [13, 14] the calculation has been extended to Next-to-NLO (NNLO). From [14], the lower limit on the mass of a charged Higgs boson $m_{H^\pm}$ is given to be about 480 GeV at 95% Confidence Level (CL) in the Type-II 2HDM when $\tan\beta$, which is the ratio of the Higgs Vacuum Expectation Values (VEVs) of the two doublets, is taken to be larger than 2. In contrast, a milder bound from $B \to X_s\gamma$ is extracted in the Type-I 2HDM, e.g., $m_{H^\pm} \gtrsim 100$ and 200 GeV when $\tan\beta = 2.5$ and 2, respectively [13], with the lower bound on $m_{H^\pm}$ weakening with increasing $\tan\beta$.

It is important to mention here that, in addition to Type-I and Type-II 2HDMs, the Type-

X and Type-Y 2HDMs can also be defined depending on the Z_2 charge assignment [15–18] and that the same bound on $m_{H^\pm}$ from $B \to X_s\gamma$ as in the Type-II (Type-I) 2HDM is obtained in the Type-Y (Type-X) 2HDM because of the identical structure of the quark Yukawa interactions. It is then interesting to consider a light charged Higgs boson scenario with $m_{H^\pm} < m_t - m_b$ in which $H^\pm$ states can be produced via a top quark decay ($t \to H^\pm b$), a channel which is being searched for at the LHC experiments. If we consider 2HDMs, such a scenario is allowed in Type-I and Type-X for $\tan\beta \gtrsim 3$ and it has been shown that the charged Higgs boson mainly decays into $\tau\nu$ in this parameter space [15, 18–20]. However, if we consider models with more than two Higgs doublets, one can find charged Higgs bosons decaying copiously into different final states.

In this paper, we investigate the phenomenology of charged Higgs bosons in 3-Higgs Doublet Models (3HDMs). Two softly-broken discrete Z_2 symmetries are imposed in order to realise the Natural Flavour Conserving (NFC) scenario, where only one of the three doublets couples to each type of fermion in order to avoid Flavour Changing Neutral Currents (FCNCs) at the tree level. Under these Z_2 symmetries, we define five independent types of Yukawa interactions in analogy with the four types of Yukawa interactions in Z_2 symmetric 2HDMs. In 3HDMs there are two physical charged Higgs bosons (denoted by $H_1^\pm$ and $H_2^\pm$, with $m_{H_1^\pm} < m_{H_2^\pm}$) and more parameters determine the phenomenology of the charged Higgs sector than in 2HDMs. In Refs. [16, 19, 21, 22], the phenomenology of $H_1^\pm$ in 3HDMs has been studied with decoupled $H_2^\pm$ in terms of effective Yukawa couplings for the down-type quark, up-type quark and charged lepton, which are expressed by a function of four independent parameters [21] in the framework of NFC. It has been shown that $H_1^\pm$ can be lighter than the top quark while satisfying constraints from $B \to X_s\gamma$ even for the case with Type-II like Yukawa couplings. Moreover, it was shown in Refs. [16, 19, 22, 23] that the decay channel $H_1^\pm \to cb$ can have a large BR (up to 80%) in a 3HDM. Although such a value is possible in the Type-Y 2HDM for $m_{H^\pm} < m_t - m_b$, the constraint $m_{H^\pm} > 480$ GeV from $B \to X_s\gamma$ rules out this scenario. Hence a large BR($H_1^\pm \to cb$) is a distinctive signature of 3HDMs.

However, there are some important shortcomings in the previous approach where the heavier charged Higgs boson is decoupled from the theory. If one takes the decoupling limit of the heavier charged Higgs boson, then the mixing angle between the two charged Higgs bosons asymptotically approaches zero because of the structure of the charged scalar

mass matrix. Eventually, this situation makes the predictions in 3HDMs identical to those in 2HDMs. In other words, the effective coupling approach [16, 19, 21, 22] is implicitly assuming that a cancellation is occurring between the contributions of the two charged Higgs bosons to $B \to X_s \gamma$, and the heavier charged Higgs boson should not be too heavy in order for sufficient cancellation to occur. Thus in this paper, we clarify the 3HDM phenomenology with a non-decoupled $H_2^\pm$ and, consequently, the impact of $H_2^\pm$ on flavour physics and its typical collider signatures have not been clarified either. We compute the BR of $B \to X_s \gamma$ at NLO in QCD in 3HDMs by taking into account both $H_1^\pm$ and $H_2^\pm$ loops, in which the dependence of the relevant five independent parameters, i.e., $m_{H_1^\pm}$, $m_{H_2^\pm}$, two ratios of VEVs and a mixing angle between $H_1^\pm$ and $H_2^\pm$, is explicitly shown with a fixed type of Yukawa interaction. We then discuss the phenomenology of $H_1^\pm$ and $H_2^\pm$ at the LHC in the parameter space allowed by $B \to X_s \gamma$ and by the direct searches for charged Higgs bosons via $t \to H^\pm b$ with $H^\pm \to \tau\nu/cs$ at the Tevatron and LHC as well as pair production $H^+ H^-$ at LEP 2. We draw attention to the fact that current LHC searches for $H^\pm$ do not have sensitivity to the region $80\,\text{GeV} < m_{H^\pm} < 90$ GeV provided that $H^\pm$ has a sizeable branching ratio to cs and/or cb, and LEP2 searches did not rule out the possibility of a $H^\pm$ in this region. We then interface these results to the standard hadro-production mode $gg, q\bar{q} \to t\bar{b}H^- +$ c.c. discussed in [24], where analytical formulae can be found.

This paper is organised as follows. In Sec. II, we define the 3HDMs. First, we give the Higgs potential under the two softly-broken discrete Z_2 symmetries and then we construct the Yukawa Lagrangian. Five types of Yukawa interactions are also defined. In Sec. III, we discuss the constraints on the parameter space from $B \to X_s \gamma$ and the direct searches for charged Higgs bosons at LEP2, Tevatron and LHC. In Sec. IV, we investigate the LHC phenomenology of the charged Higgs bosons. Conclusions are given in Sec. V. In Appendix A, we present the formulae for the mass matrices of the charged, CP-odd and CP-even Higgs bosons. In Appendix B, we summarise all the SM input parameters which are used for the numerical analysis of this paper.

II. MODELS

We discuss extensions of the SM Higgs sector with three isospin doublet Higgs fields Φ_i ($i = 1$-3), where all the Higgs fields have non-zero VEVs. In general, each of these Higgs

	Φ_1	Φ_2	Φ_3	u_R	d_R	e_R	$Q_L,\, L_L$	$\Phi_u\ \Phi_d\ \Phi_e$
Type-I	$(+,+)$	$(+,-)$	$(-,+)$	$(+,-)$	$(+,-)$	$(+,-)$	$(+,+)$	$\Phi_2\ \Phi_2\ \Phi_2$
Type-II	$(+,+)$	$(+,-)$	$(-,+)$	$(+,-)$	$(+,+)$	$(+,+)$	$(+,+)$	$\Phi_2\ \Phi_1\ \Phi_1$
Type-X	$(+,+)$	$(+,-)$	$(-,+)$	$(+,-)$	$(+,-)$	$(+,+)$	$(+,+)$	$\Phi_2\ \Phi_2\ \Phi_1$
Type-Y	$(+,+)$	$(+,-)$	$(-,+)$	$(+,-)$	$(+,+)$	$(+,-)$	$(+,+)$	$\Phi_2\ \Phi_1\ \Phi_2$
Type-Z	$(+,+)$	$(+,-)$	$(-,+)$	$(+,-)$	$(+,+)$	$(-,+)$	$(+,+)$	$\Phi_2\ \Phi_1\ \Phi_3$

TABLE I: Charge assignments under the $Z_2 \times \tilde{Z}_2$ symmetry, e.g. $(+,-)$ means Z_2-even and $\tilde{Z}_2$-odd.

	Factor for $\tilde{H}_1$, $\tilde{A}_1$ and $\tilde{H}_1^\pm$			Factor for $\tilde{H}_2$, $\tilde{A}_2$ and $\tilde{H}_2^\pm$		
	R_{u2}/R_{u1}	R_{d2}/R_{d1}	R_{e2}/R_{e1}	R_{u3}/R_{u1}	R_{d3}/R_{d1}	R_{e3}/R_{e1}
Type-I	$\cot\beta$	$\cot\beta$	$\cot\beta$	0	0	0
Type-II	$\cot\beta$	$-\tan\beta$	$-\tan\beta$	0	$-\tan\gamma/\cos\beta$	$-\tan\gamma/\cos\beta$
Type-X	$\cot\beta$	$\cot\beta$	$-\tan\beta$	0	0	$-\tan\gamma/\cos\beta$
Type-Y	$\cot\beta$	$-\tan\beta$	$\cot\beta$	0	$-\tan\gamma/\cos\beta$	0
Type-Z	$\cot\beta$	$-\tan\beta$	$-\tan\beta$	0	$-\tan\gamma/\cos\beta$	$\cot\gamma/\cos\beta$

TABLE II: Factors appearing in Eq. (16) for each type of Yukawa interaction.

doublets would couple to all three types of fermions, i.e., up- and down-type quarks and charged leptons. However, this structure causes FCNCs at the tree level, as is well known in the general 2HDM without discrete Z_2 symmetries. The easiest way to avoid FCNCs is to consider a Yukawa Lagrangian where each of the three Higgs doublets couples to at most one of the fermion types, and such a Lagrangian takes the following form:

$$-\mathcal{L}_Y = Y_u \bar{Q}_L (i\sigma_2) \Phi_u^* u_R + Y_d \bar{Q}_L \Phi_d d_R + Y_e \bar{L}_L \Phi_e e_R + \text{h.c.}, \tag{1}$$

where $\Phi_{u,d,e}$ are either Φ_1, Φ_2 or Φ_3.

We can naturally realise the above Lagrangian by imposing two discrete symmetries Z_2 and $\tilde{Z}_2$ on the Higgs sector. In general, we can also introduce soft-breaking Z_2 and $\tilde{Z}_2$ terms in the Higgs potential without losing the key property of the absence of FCNCs at tree level. Depending on the charge assignment of the Z_2 and $\tilde{Z}_2$ symmetries, we can define

five independent types of Yukawa interactions[1] as listed in Tab. I. We note that the Type-Z corresponds to the Yukawa interaction of the 3HDM discussed in Ref. [21] which is named therein as the 'democratic 3HDM'.

The most general Higgs potential under the $SU(2)_L \times U(1)_Y \times Z_2 \times \tilde{Z}_2$ symmetry is given by

$$V(\Phi_1, \Phi_2, \Phi_3) = \sum_{i=1}^{3} \mu_i^2 \Phi_i^\dagger \Phi_i - (\mu_{12}^2 \Phi_1^\dagger \Phi_2 + \mu_{13}^2 \Phi_1^\dagger \Phi_3 + \mu_{23}^2 \Phi_2^\dagger \Phi_3 + \text{h.c.})$$
$$+ \frac{1}{2} \sum_{i=1}^{3} \lambda_i (\Phi_i^\dagger \Phi_i)^2 + \rho_1 (\Phi_1^\dagger \Phi_1)(\Phi_2^\dagger \Phi_2) + \rho_2 |\Phi_1^\dagger \Phi_2|^2 + \frac{1}{2} [\rho_3 (\Phi_1^\dagger \Phi_2)^2 + \text{h.c.}]$$
$$+ \sigma_1 (\Phi_1^\dagger \Phi_1)(\Phi_3^\dagger \Phi_3) + \sigma_2 |\Phi_1^\dagger \Phi_3|^2 + \frac{1}{2} [\sigma_3 (\Phi_1^\dagger \Phi_3)^2 + \text{h.c.}]$$
$$+ \kappa_1 (\Phi_2^\dagger \Phi_2)(\Phi_3^\dagger \Phi_3) + \kappa_2 |\Phi_2^\dagger \Phi_3|^2 + \frac{1}{2} [\kappa_3 (\Phi_2^\dagger \Phi_3)^2 + \text{h.c.}], \tag{2}$$

where the μ_{12}^2, μ_{13}^2 and μ_{23}^2 terms are the soft-breaking terms for Z_2 and $\tilde{Z}_2$. In general, μ_{ij}^2, ρ_3, σ_3 and κ_3 are complex parameters but throughout the paper we take them to be real for simplicity, thereby avoiding explicit CP violation. Of the 18 free parameters in the 3HDM scalar potential, two are fixed by the mass of the W boson and the mass of the discovered neutral Higgs boson. There are theoretical constraints on the 16 remaining parameters from requiring stability of the vacuum, absence of charge breaking minima, compliance with unitarity of scattering processes etc. Such constraints are well-known in the 2HDM (e.g. see [25]) for a recent study) and have also been discussed for the scalar potential in 3HDMs [26–30]. We do not impose these constraints because they only rule out certain regions of the parameter space of 16 variables, which might not include the region what we are interested in for the phenomenological study focusing on the charged Higgs sector. As we will see below, the phenomenology in the charged Higgs sector depends on only 5 parameters (which we take as unconstrained parameters), and we will assume that the freedom in the other 11 parameters can be used to comply with the above theoretical constraints. To justify this approach we note that the analogous constraints on the scalar potential in 2HDMs do not constrain the two parameters in the charged Higgs sector ($m_{H^\pm}$ and $\tan\beta$) due to the freedom in the remaining four parameters (for the case of a 2HDM with a softly-broken Z_2 symmetry).

---

[1] We can also define additional four types by interchanging $\Phi_1 \leftrightarrow \Phi_3$. However, these types are physically identical to the last four types given in Tab. I.

The three Higgs doublet fields can be parameterised by

$$\Phi_i = \begin{bmatrix} \omega_i^+ \\ \frac{1}{\sqrt{2}}(h_i + v_i + iz_i) \end{bmatrix}, \quad (i = 1, ...3), \tag{3}$$

where the v_i's are the VEVs of the Φ_i's with the sum rule $\sum_i v_i^2 \equiv v^2 = 1/(\sqrt{2}G_F) \simeq (246$ GeV$)^2$. It is convenient to define the so-called Higgs basis in 3HDMs, in which only one of the three doublets contains the VEV v and the Nambu-Goldstone (NG) bosons. This can be defined by introducing the orthogonal 3×3 matrix R as

$$\begin{pmatrix} \Phi_1 \\ \Phi_2 \\ \Phi_3 \end{pmatrix} = R \begin{pmatrix} \Phi \\ \Psi_1 \\ \Psi_2 \end{pmatrix}. \tag{4}$$

The R matrix is expressed in terms of the three VEVs:

$$R = \begin{pmatrix} \frac{v_1}{v} & -\frac{v_2 v_1}{v_{13} v} & -\frac{v_3}{v_{13}} \\ \frac{v_2}{v} & \frac{v_{13}}{v} & 0 \\ \frac{v_3}{v} & -\frac{v_2 v_3}{v_{13} v} & \frac{v_1}{v_{13}} \end{pmatrix} = \begin{pmatrix} \cos\gamma & 0 & -\sin\gamma \\ 0 & 1 & 0 \\ \sin\gamma & 0 & \cos\gamma \end{pmatrix} \begin{pmatrix} \cos\beta & -\sin\beta & 0 \\ \sin\beta & \cos\beta & 0 \\ 0 & 0 & 1 \end{pmatrix}$$

$$= \begin{pmatrix} \cos\beta\cos\gamma & -\sin\beta\cos\gamma & -\sin\gamma \\ \sin\beta & \cos\beta & 0 \\ \cos\beta\sin\gamma & -\sin\beta\sin\gamma & \cos\gamma \end{pmatrix}, \tag{5}$$

where we introduced the two ratios of the VEVs as follows

$$\tan\beta \equiv \frac{v_2}{v_{13}}, \quad \tan\gamma \equiv \frac{v_3}{v_1}, \quad \text{with} \quad v_{13} \equiv \sqrt{v_1^2 + v_3^2}. \tag{6}$$

Using this notation, each of the VEVs is expressed by

$$v_1 = v_{13}\cos\gamma = v\cos\beta\cos\gamma, \quad v_2 = v\sin\beta, \quad v_3 = v_{13}\sin\gamma = v\cos\beta\sin\gamma. \tag{7}$$

We note that these definitions differ from those used in Ref. [21]. In the Higgs basis, the three doublets Φ, Ψ_1 and Ψ_2 are expressed by

$$\Phi = \begin{pmatrix} G^+ \\ \frac{v + \tilde{h} + iG^0}{\sqrt{2}} \end{pmatrix}, \quad \Psi_a = \begin{pmatrix} \tilde{H}_a^+ \\ \frac{\tilde{H}_a + i\tilde{A}_a}{\sqrt{2}} \end{pmatrix} \quad \text{with} \quad a = 1, 2, \tag{8}$$

where $G^\pm$ and G^0 are the NG bosons which are absorbed into the longitudinal components of W and Z, respectively. In Eq. (8), two singly-charged states $\tilde{H}_a^\pm$, two CP-odd states

7

$\tilde{A}_a$ and three CP-even states $\tilde{h}$ and $\tilde{H}_a$ are not in general the mass eigenstates. The mass eigenstates for the singly-charged ($H_1^\pm$ and $H_2^\pm$) and the CP-odd states (A_1 and A_2) are defined by

$$\begin{pmatrix} \tilde{H}_1^\pm \\ \tilde{H}_2^\pm \end{pmatrix} = \begin{pmatrix} \cos\theta_C & -\sin\theta_C \\ \sin\theta_C & \cos\theta_C \end{pmatrix} \begin{pmatrix} H_1^\pm \\ H_2^\pm \end{pmatrix}, \quad \begin{pmatrix} \tilde{A}_1 \\ \tilde{A}_2 \end{pmatrix} = \begin{pmatrix} \cos\theta_A & -\sin\theta_A \\ \sin\theta_A & \cos\theta_A \end{pmatrix} \begin{pmatrix} A_1 \\ A_2 \end{pmatrix}, \tag{9}$$

where the mixing angles θ_C and θ_A are expressed in terms of the mass matrix elements for the singly charged states ($\mathcal{M}_C^2$) and those for the CP-odd states ($\mathcal{M}_A^2$) in the Higgs basis (see Appendix A):

$$\tan 2\theta_C = \frac{2(\mathcal{M}_C^2)_{12}}{(\mathcal{M}_C^2)_{11} - (\mathcal{M}_C^2)_{22}}, \quad \tan 2\theta_A = \frac{2(\mathcal{M}_A^2)_{12}}{(\mathcal{M}_A^2)_{11} - (\mathcal{M}_A^2)_{22}}. \tag{10}$$

The squared mass eigenvalues for the singly-charged and CP-odd Higgs bosons are given by

$$m_{H_1^\pm}^2 = (\mathcal{M}_C^2)_{11} \cos^2\theta_C + (\mathcal{M}_C^2)_{22} \sin^2\theta_C + (\mathcal{M}_C^2)_{12} \sin 2\theta_C, \tag{11}$$

$$m_{H_2^\pm}^2 = (\mathcal{M}_C^2)_{11} \sin^2\theta_C + (\mathcal{M}_C^2)_{22} \cos^2\theta_C - (\mathcal{M}_C^2)_{12} \sin 2\theta_C, \tag{12}$$

$$m_{A_1}^2 = (\mathcal{M}_A^2)_{11} \cos^2\theta_A + (\mathcal{M}_A^2)_{22} \sin^2\theta_A + (\mathcal{M}_A^2)_{12} \sin 2\theta_A, \tag{13}$$

$$m_{A_2}^2 = (\mathcal{M}_A^2)_{11} \sin^2\theta_A + (\mathcal{M}_A^2)_{22} \cos^2\theta_A - (\mathcal{M}_A^2)_{12} \sin 2\theta_A. \tag{14}$$

For the CP-even states, there are three physical states, so that we need to diagonalise the 3×3 mass matrix to obtain the mass eigenvalues. The mass eigenstates are defined by introducing the 3×3 orthogonal matrix R_H as

$$\begin{pmatrix} \tilde{h} \\ \tilde{H}_1 \\ \tilde{H}_2 \end{pmatrix} = R_H \begin{pmatrix} h \\ H_1 \\ H_2 \end{pmatrix}. \tag{15}$$

Among the three mass eigenstates, one of them must be identified as the discovered Higgs boson at the LHC with a mass of about 125 GeV, which in our case is the h state. The mass matrix for the CP-even states in the Higgs basis ($\tilde{h}, \tilde{H}_1, \tilde{H}_2$) is also given in Appendix A.

The Yukawa interaction terms can be expressed in the Higgs basis as

$$-\mathcal{L}_Y = \sum_{f=u,d,e} \frac{m_{f^i}}{v} \bar{f}^i \left[\left(\tilde{h} + \frac{R_{f2}}{R_{f1}} \tilde{H}_1 + \frac{R_{f3}}{R_{f1}} \tilde{H}_2 \right) - 2I_f \left(\frac{R_{f2}}{R_{f1}} \tilde{A}_1 + \frac{R_{f3}}{R_{f1}} \tilde{A}_2 \right) \gamma_5 \right] f^i$$

$$+ \frac{\sqrt{2}}{v} \left[\bar{u}^j V_{ji} m_{d^i} \left(\frac{R_{d2}}{R_{d1}} \tilde{H}_1^+ + \frac{R_{d3}}{R_{d1}} \tilde{H}_2^+ \right) P_R d^i - \bar{u}^i m_{u^i} V_{ij} \left(\frac{R_{u2}}{R_{u1}} \tilde{H}_1^+ + \frac{R_{u3}}{R_{u1}} \tilde{H}_2^+ \right) P_L d^j \right] + \text{h.c.}$$

$$+ \frac{\sqrt{2}}{v} \bar{\nu}^i m_{e^i} \left(\frac{R_{e2}}{R_{e1}} \tilde{H}_1^+ + \frac{R_{e3}}{R_{e1}} \tilde{H}_2^+ \right) P_R e^i + \text{h.c.} \tag{16}$$
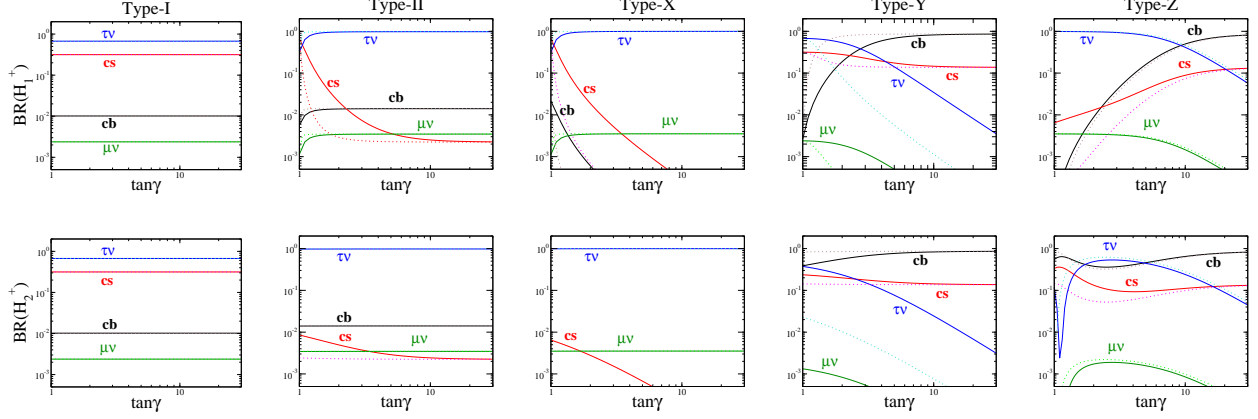
FIG. 1: Branching ratios of $H_1^\pm$ (upper panels) and $H_2^\pm$ (lower panels) as a function of $\tan\gamma$ in the Type-I, II, X, Y and Z 3HDM from the left to right panels. We take $m_{H_1^\pm} = 100$ GeV, $m_{H_2^\pm} = 150$ GeV and $\theta_C = -\pi/4$. The value of $\tan\beta$ is taken to be 2 (5) for the solid (dotted) curves.

where $I_f = +1/2\,(-1/2)$ for $f = u\,(d,e)$ and V_{ij} is the Cabibbo-Kobayashi-Maskawa (CKM) matrix element. The ratios of the matrix elements R_{f2}/R_{f1} and R_{f3}/R_{f1} $(f = u, d, e)$ are given in Tab. II for each of the five types of Yukawa interactions. Here, it is useful to show the correspondence between the X_a, Y_a and Z_a couplings used in Refs. [16, 19, 21, 22] and the above couplings. When we define these couplings by

$$-\mathcal{L}_Y = \frac{\sqrt{2}}{v} \sum_{a=1,2} \left(\bar{u}^j V_{ji} m_{d^i} X_a P_R d^i + \bar{u}^i m_{u^i} V_{ij} Y_a P_L d^j + \bar{\nu}^i m_{e^i} Z_a P_R e^i \right) H_a^+ + \text{h.c.}, \quad (17)$$

we find

$$X_1 = \frac{R_{d2}}{R_{d1}}c_C + \frac{R_{d3}}{R_{d1}}s_C, \;\; Y_1 = -\frac{R_{u2}}{R_{u1}}c_C - \frac{R_{u3}}{R_{u1}}s_C, \;\; Z_1 = \frac{R_{e2}}{R_{e1}}c_C + \frac{R_{e3}}{R_{e1}}s_C, \quad (18)$$

$$X_2 = -\frac{R_{d2}}{R_{d1}}s_C + \frac{R_{d3}}{R_{d1}}c_C, \;\; Y_2 = \frac{R_{u2}}{R_{u1}}s_C - \frac{R_{u3}}{R_{u1}}c_C, \;\; Z_2 = -\frac{R_{e2}}{R_{e1}}s_C + \frac{R_{e3}}{R_{e1}}c_C, \quad (19)$$

where $s_C = \sin\theta_C$ and $c_C = \cos\theta_C$. In this paper, we particularly focus on the physics related to the charged Higgs bosons $H_1^\pm$ and $H_2^\pm$, for which the number of relevant (new physics) parameters is five, namely,

$$m_{H_1^\pm}, \;\; m_{H_2^\pm}, \;\; \tan\beta, \;\; \tan\gamma, \;\; \text{and} \;\; \theta_C. \quad (20)$$

A sixth parameter [21], which is a complex phase δ of the mass matrix $\mathcal{M}_C^2$, is set to be zero as we have already assumed the CP-invariance of the Higgs sector.
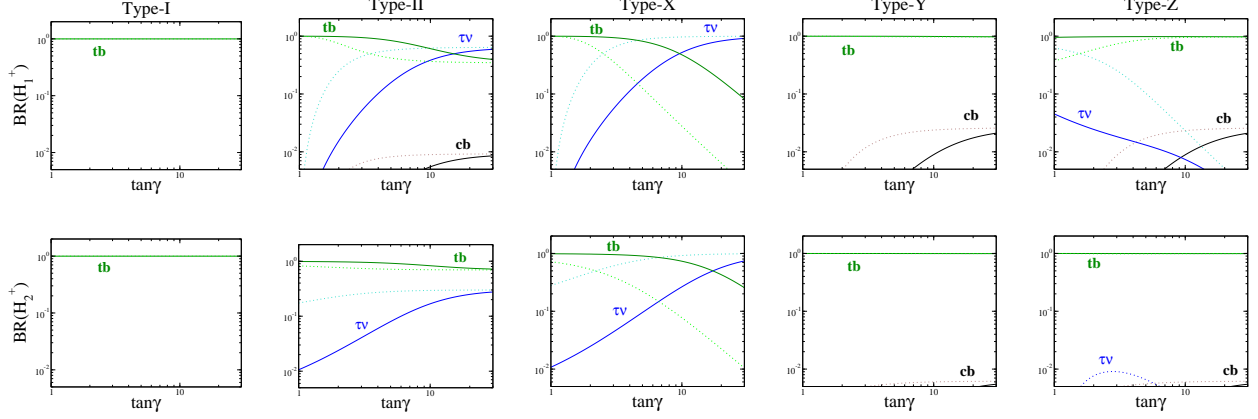
FIG. 2: Branching ratios of $H_1^\pm$ (upper panels) and $H_2^\pm$ (lower panels) as a function of $\tan\gamma$ in the Type-I, II, X, Y and Z 3HDM from the left to right panels. We take $m_{H_1^\pm} = 200$ GeV, $m_{H_2^\pm} = 250$ GeV and $\theta_C = -\pi/4$. The value of $\tan\beta$ is taken to be 2 (5) for the solid (dotted) curves.

We now show the BRs of $H_1^\pm$ and $H_2^\pm$ in the Type-I, Type-II, Type-X, Type-Y and Type-Z 3HDMs. For simplicity, we take all the masses of extra neutral Higgs bosons ($H_{1,2}$ and $A_{1,2}$) to be larger than those of the charged Higgs bosons and take the alignment limit $R_H \to I_{3\times3}$, where the CP-even states in the Higgs basis $\tilde{h}$ and $\tilde{H}_{1,2}$ correspond to the mass eigenstates. In this case, the decays of the charged Higgs bosons such as $H_a^\pm \to W^{(*)\pm}A_a/H_a/h$ ($a = 1, 2$) do not appear nor do the $H_2^\pm \to H_1^\pm H_a/h$ ($a = 1, 2$) ones either[2]. As a result, only the charged Higgs boson decays into fermion pairs need to be considered. The leading order expressions for the partial widths of $H_1^\pm$ and $H_2^\pm$ decaying to fermions are given by:

$$\Gamma(H_a^\pm \to \ell^\pm\nu) = \frac{G_F m_{H_a^\pm}}{4\pi\sqrt{2}} m_\ell^2 Z_a^2 \left(1 - \frac{m_\ell^2}{m_{H_a^\pm}^2}\right)^2, \tag{21}$$

$$\Gamma(H_a^\pm \to ud) = \frac{3G_F |V_{ud}|^2 m_{H_a^\pm}}{4\pi\sqrt{2}}$$
$$\times \left[(\bar{m}_d^2 X_a^2 + \bar{m}_u^2 Y_a^2)(1 - x_u^a - x_d^a) - 4\bar{m}_u\bar{m}_d\sqrt{x_u^a x_d^a} X_a Y_a\right] \lambda^{1/2}(x_u, x_d), \tag{22}$$

where $\bar{m}_u$ and $\bar{m}_d$ are the running quark masses evaluated at the scale of the mass of the

---

[2] There is no $H_1^\pm H_2^\mp Z$ vertex at tree level because both charged Higgs bosons originate from Higgs fields with identical $SU(2)_L \times U(1)_Y$ charge. Thus, there is no $H_2^\pm \to H_1^\pm Z^{(*)}$ decay at the tree level either. We also note that there is no $H_1^\pm H_2^\mp \gamma$ vertex in any models with singly charged Higgs bosons at any order of perturbation theory because of a Ward identity.

charged Higgs bosons. When calculating the running masses we fix the scale to be 100 GeV, since using the actual charged Higgs boson masses only leads to small numerical differences from the values obtained when taking the scale to be 100 GeV. The parameters m_u^{pole} and m_d^{pole} are the pole masses of quarks, and $x_u^a = (m_u^{\text{pole}})^2/m_{H_a^\pm}^2$ and $x_d^a = (m_d^{\text{pole}})^2/m_{H_a^\pm}^2$. The values of all these quark masses are given in Appendix B. In the above expression, λ is the two body phase space function given by $\lambda(x, y) = 1 + x^2 + y^2 - 2x - 2y - 2xy$.

In Fig. 1, we show the BRs of $H_1^\pm$ (upper panels) and $H_2^\pm$ (lower panels) as a function of $\tan\gamma$. In these plots, we take $m_{H_1^\pm} = 100$ GeV, $m_{H_2^\pm} = 150$ GeV and $\theta_C = -\pi/4$. The solid and dotted curves show the case for $\tan\beta = 2$ and 5, respectively. We see that, in the Type-I, Type-II and Type-X 3HDM, the decays of the charged Higgs bosons into $\tau\nu$ pairs are dominant. In contrast, in the Type-Y and Type-Z 3HDM, the decay into cb can be dominant in the large $\tan\gamma$ region. As shown in [16, 19, 22], the parameter space of a large BR of the cb channel corresponds to $|X_a| \gg |Y_a|, |Z_a|$ (see Eq. (21) and Eq. (22)) and we have shown that this condition can only be realised in the Type-Y and Type-Z 3HDM.

We show similar plots in Fig. 2, but we here take $m_{H_1^\pm} = 200$ GeV, $m_{H_2^\pm} = 250$ GeV and $\theta_C = -\pi/4$. Except for the Type-X 3HDM, the decay of the charged Higgs bosons into tb is dominant in wide regions of the parameter space. In the Type-Y and Type-Z 3HDM, the BR of the cb mode can be at the few percent level in the large $\tan\gamma$ region.

From these results, it can be seen that the charged Higgs boson decay into cb can be important in the Type-Y and Type-Z 3HDMs, especially when the charged Higgs boson masses are below the top mass. We would finally like to emphasise that the $H_{1,2}^\pm \to cb$ decay can be a useful tool to distinguish 3HDMs from 2HDMs because of the following reason. In practice, in the 2HDM with a softly-broken Z_2 symmetry, the $H^\pm \to cb$ decay can be dominant when $m_{H^\pm} < m_t - m_b$ and $\tan\beta \gtrsim 3$ for the Type-Y case [18, 19]. However, such a light charged Higgs boson is excluded by the $B \to X_s\gamma$ data. In our model, the constraint from $B \to X_s\gamma$ is instead avoidable using a cancellation between the contributions from the loops involving $H_1^\pm$ and $H_2^\pm$ as we will clarify in the next section.

III. CONSTRAINTS FROM $B \to X_s\gamma$ AND DIRECT SEARCHES

In this section, we first discuss the constraints on the parameter space of the five types of 3HDMs from measurements of $B \to X_s\gamma$. Then we move on to consider constraints from

direct searches for $H_1^\pm$ and $H_2^\pm$ at colliders.

A. Flavour sector limits

We calculate the branching fraction of the radiative $B \to X_s\gamma$ decay process at NLO in QCD. In our model, in addition to the $W^\pm$ boson loop contribution, $H_1^\pm$ and $H_2^\pm$ also contribute to this process at the same perturbative level. The decay rate of $B \to X_s\gamma$ can be written as a sum of the following three parts: i) the b quark decay process $b \to s\gamma$ ($\Gamma_{b\to s\gamma}$); ii) the gluon bremsstrahlung process $b \to s\gamma g$ ($\Gamma_{b\to s\gamma g}$); iii) non-perturbative effects due to the mesonic processes ($\Gamma_{\text{non-pert.}}$). Thus,

$$\Gamma(B \to X_s\gamma) = \Gamma_{b\to s\gamma} + \Gamma_{b\to s\gamma g} + \Gamma_{\text{non-pert.}}. \tag{23}$$

The first and the second contribution depend on the new physics parameters such as the charged Higgs boson masses and their couplings to quarks, while the third contribution does not. The decay rates $\Gamma_{b\to s\gamma}$ and $\Gamma_{b\to s\gamma g}$ are calculated using the Wilson coefficients at a scale μ [31]:

$$C_i^{\text{eff}}(\mu, m_{H_1^\pm}, m_{H_2^\pm}) = C_{i,\text{SM}}^{\text{eff}}(\mu) + \sum_{a=1,2} \left[(X_a Y_a^*) C_{i,XY}^{\text{eff}}(\mu, m_{H_a^\pm}) + |Y_a|^2 C_{i,YY}^{\text{eff}}(\mu, m_{H_a^\pm}) \right], \tag{24}$$

where $i = 1, \ldots 8$ while X_a and Y_a ($a = 1, 2$) are given in Eqs. (18) and (19). We note that the results of the 2HDMs can be reproduced by taking the limit of $\theta_C \to 0$ or $m_{H_2^\pm} \to m_{H_1^\pm}$. The latter holds due to the sum rule:

$$\sum_{a=1,2} X_a Y_a = X_1 Y_1 \Big|_{\theta_C=0}, \quad \sum_{a=1,2} |Y_a|^2 = |Y_1|^2 \Big|_{\theta_C=0}. \tag{25}$$

The structure of the quark Yukawa couplings are the same in Type-II, Type-Y and Type-Z 3HDMs and so the same bound from $B \to X_s\gamma$ applies equally to these three models. Likewise, the bound from $B \to X_s\gamma$ applies equally to the Type-I and Type-X 3HDMs. To obtain $\Gamma_{b\to s\gamma}$ and $\Gamma_{b\to s\gamma g}$, we set the scale μ appearing in Eq. (24) to be the bottom quark mass scale μ_b. All the Wilson coefficients that are calculated at the matching scale $\mu = \mu_W$ have to be evaluated at μ_b by solving the renormalisation group equations. In Ref. [11], all the relevant Wilson coefficients at $\mu = \mu_b$ at LO and NLO are given in terms of those at $\mu = \mu_W$ and we adopt them for our numerical evaluations. Using the decay rate and BR of
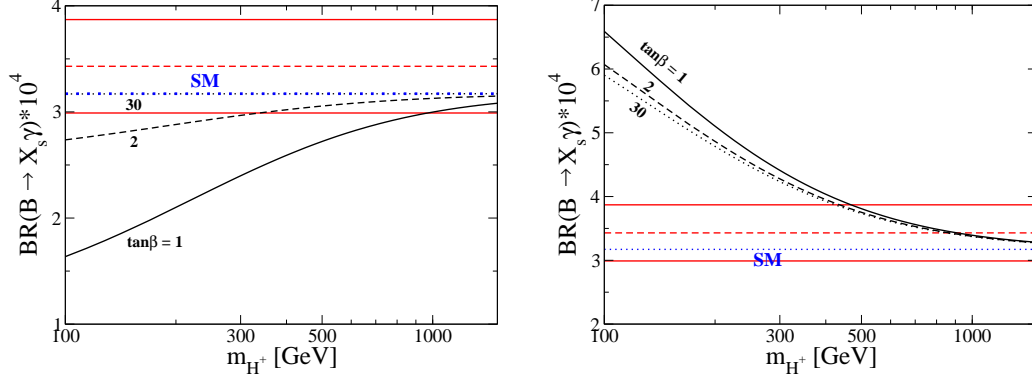
12

FIG. 3: Predictions for the branching ratio of the $B \to X_s\gamma$ process in the Type-I (left) and Type-II 2HDM (right) as a function of $m_{H^\pm}$. We take $\tan\beta = 1$ (solid), 2 (dashed) and 30 (dotted). The red solid (dashed) lines are the 2σ allowed region (central value) of the experimental result. The blue dotted line is the SM prediction.

the semi-leptonic decay of the B meson, we can express the BR of the $B \to X_s\gamma$ process as

$$\mathrm{BR}(B \to X_s\gamma) = \frac{\Gamma(B \to X_s\gamma)}{\Gamma(B \to X_c\ell\nu)}\mathrm{BR}(B \to X_c\ell\nu). \tag{26}$$

The measured value of the BR is given [32] as

$$\mathrm{BR}(B \to X_s\gamma) = (3.43 \pm 0.22) \times 10^{-4}. \tag{27}$$

All the SM input parameters for the numerical calculations are listed in Appendix B, and we take $\mu_b = m_b^{\mathrm{pole}}$ and $\mu_W = m_{W^\pm}$.

In order to compare the predictions in 2HDMs with those in 3HDMs, we first show the results in the former case where we have only one pair of charged Higgs bosons $H^\pm$. In Fig. 3, we show the prediction of the BR of $B \to X_s\gamma$ in the Type-I (left) and Type-II (right) 2HDM as a function of the mass of the charged Higgs boson $m_{H^\pm}$. The SM prediction is indicated as the blue dotted line. The 2σ bounds from the experimental data are shown as horizontal red solid lines. The black curves show the results in 2HDMs with several fixed values of $\tan\beta$. We can see that the $H^\pm$ contribution interferes destructively (constructively) with the SM contribution in the Type-I (Type-II) 2HDM. In addition, in Type-I, when we take a large $\tan\beta$ value, the $H^\pm$ contribution becomes quite small because all the $H^\pm$ couplings to quarks are proportional to $\cot\beta$. In contrast, in the Type-II case, even if we take a large $\tan\beta$ value, the $H^\pm$ loop effect does not vanish. This can be understood by noting that the
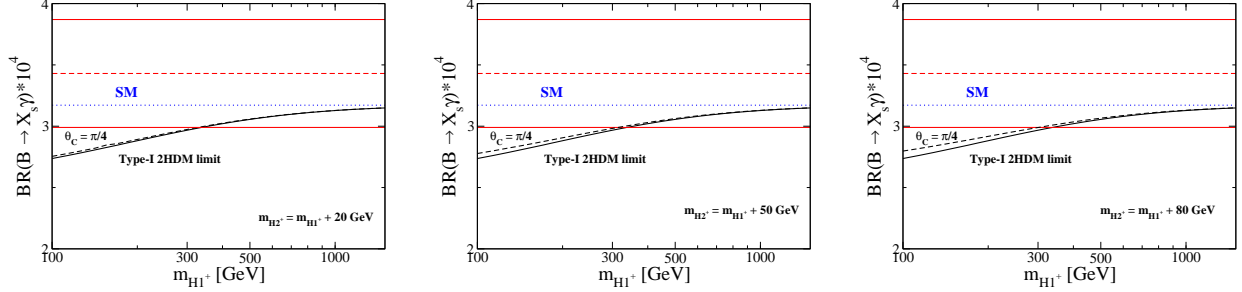
FIG. 4: Prediction of the branching ratio of $B \to X_s \gamma$ in the Type-I 3HDM (black dashed curve) with $\tan \beta = 2$ and $\theta_C = \pi/4$ as a function of $m_{H_1^\pm}$. As a comparison, we also show the results in the Type-I 2HDM with $\tan \beta = 2$ as the black solid curve. The left, centre and right panels show the case for $m_{H_2^\pm} - m_{H_1^\pm} = 20$, 50 and 80 GeV, respectively. The same results are obtained in the Type-X 3HDM.

coupling product $X_1 Y_1^*$ with $\theta_C \to 0$ appearing in the Wilson coefficient is equal to unity in the Type-II 2HDM. Consequently, in Type-I, a severe lower limit on $m_{H^\pm}$ is only obtained for small values of $\tan \beta$, with the bound being about $m_{H^\pm} > 1$ TeV with $\tan \beta = 1$. In Type-II, when $\tan \beta \gtrsim 2$, we obtain $m_{H^\pm} \gtrsim 450$ GeV independently of $\tan \beta$[3].

Next, we show the numerical results of $\mathrm{BR}(B \to X_s \gamma)$ in 3HDMs. In Fig. 4, the $m_{H_1^\pm}$ dependence of $\mathrm{BR}(B \to X_s \gamma)$ in the Type-I 3HDM is shown as the black dashed curve. The prediction in the Type-I 2HDM is also shown as the solid curve for comparison. In these plots, we take $\tan \beta = 2$ and $\theta_C = \pi/4$. The mass difference $m_{H_2^\pm} - m_{H_1^\pm}$ is taken to be 20 (left panel), 50 (centre panel) and 80 GeV (right panel). We can see that the difference between the prediction in the Type-I 3HDM and the Type-I 2HDM becomes slightly bigger as the mass difference $m_{H_2^\pm} - m_{H_1^\pm}$ increases, but, even for the case of $m_{H_2^\pm} - m_{H_1^\pm} = 80$ GeV, these two results are almost the same. We note that $\mathrm{BR}(B \to X_s \gamma)$ does not depend on $\tan \gamma$ in the Type-I 3HDM, because $\tan \gamma$ is not entering the quark Yukawa couplings as shown in Tab. II. We also note that the prediction in the Type-I 3HDM does not depend on the sign of θ_C.

---

[3] In Ref. [14], the calculation at NNLO in QCD has been evaluated in the Type-II 2HDM and the slightly more stringent limit $m_{H^\pm} \gtrsim 480$ GeV has been derived at 95% CL.
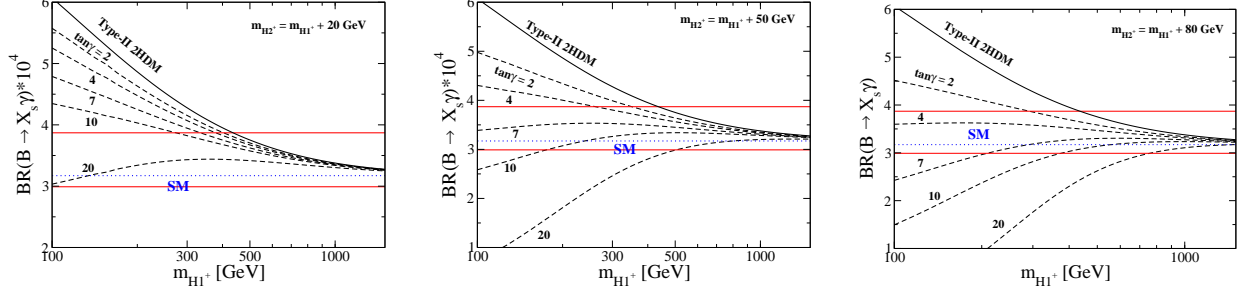
14

FIG. 5: Prediction of the branching ratio of $B \to X_s\gamma$ in the Type-II 3HDM with several values of $\tan\gamma$. We take $\tan\beta = 2$ and $\theta_C = -\pi/4$. As a comparison, we also show the results in the Type-II 2HDM with $\tan\beta = 2$ as the black solid curve. The left, centre and right panels show the case for $m_{H_2^\pm} - m_{H_1^\pm} = 20$, 50 and 80 GeV, respectively. The same results are obtained in the Type-Y and Type-Z 3HDM.

In Fig. 5, the $m_{H_1^\pm}$ dependence of $\mathrm{BR}(B \to X_s\gamma)$ in the Type-II 3HDM for several fixed values of $\tan\gamma$ is shown as black dashed curves. The prediction in the Type-II 2HDM is also shown as the solid curve for comparison. In these plots, we take $\tan\beta = 2$ and $\theta_C = -\pi/4$. The mass difference $m_{H_2^\pm} - m_{H_1^\pm}$ is taken to be 20, 50 and 80 GeV in the left, centre and right panel, respectively. It is clear that the prediction in the 3HDM becomes smaller when we take a larger value of $\tan\gamma$. This tendency becomes more evident with larger mass differences. As a result, we can find that cases where both charged Higgs boson masses of $\mathcal{O}(100)$ GeV are allowed by taking appropriate values for $\tan\gamma$ and their mass difference.

We here comment on the constraint on the parameter space from the other observables in flavour physics according to Ref. [21]. We note that the constraints discussed in Ref. [21] are based on a 3HDM with $H_2^\pm$ decoupled, so that we cannot simply apply them to our case. In the following, we apply these constraints to get the limit on each of the couplings for $H_1^\pm$ and $H_2^\pm$, which means that we do not take into account the interference effect of the two charged Higgs boson contributions.

From R_b measured from the $Z \to b\bar{b}$ decay, we obtain

$$|Y_a| \leq 0.72 + 0.24 \left(\frac{m_{H_1^\pm}}{100 \text{ GeV}} \right) \quad \text{at 95\% CL,} \tag{28}$$

under $|X_a| < 50$ $(a = 1, 2)$. This can be easily avoided by taking $\tan\beta \gtrsim 1$ for $m_{H_1^\pm} = 100$ GeV. The bound on the charged lepton coupling Z_1 is obtained from the leptonic τ decay

as

$$Z_a \leq 40 \left(\frac{m_{H_1^\pm}}{100 \text{ GeV}} \right) \quad \text{at 95\% CL.} \tag{29}$$

This corresponds to the bound on $\tan\gamma \lesssim 32(15)$ for $\tan\beta = 2(5)$ with $m_{H_1^\pm} = 100$ GeV and $\theta_C = -\pi/4$ in the Type-II and Type-X 3HDMs. For the other types, this does not set an upper limit on $\tan\gamma$ unless we take $\tan\beta \gg 1$ and/or $m_{H_1^\pm} \ll 100$ GeV. Finally, from the measurement of $B \to \tau\nu$, we obtain

$$|X_a Z_a| \leq 1080 \left(\frac{m_{H_1^\pm}}{100 \text{ GeV}} \right)^2 \quad \text{at 95\% CL.} \tag{30}$$

This gives an important constraint on the parameters only in the Type-II 3HDM, because both X_1 and Z_1 are enhanced by increasing $\tan\beta$ and $\tan\gamma$. For example, $\tan\gamma \gtrsim 22(11)$ is excluded when $\tan\beta = 2(5)$, $m_{H_1^\pm} = 100$ GeV and $\theta_C = -\pi/4$. We checked that all these above constraints are satisfied in the numerical analysis presented in the succeeding sections.

B. Collider limits

As discussed in the previous subsection, in 3HDMs, we can take the charged Higgs boson masses to be $\mathcal{O}(100)$ GeV without conflict with the $B \to X_s\gamma$ data. In this subsection we discuss this scenario at the LHC as a hallmark manifestation of a 3HDM, particularly for the Type-Y and Type-Z cases, because the characteristic decay of the charged Higgs bosons $H_{1,2}^\pm \to cb$ can be dominant.

When we consider the case for $m_{H_{1,2}^\pm} < m_t - m_b$, we need to take into account the constraints from direct searches for $H^\pm$ states from the top quark decay $t \to H^\pm b$ at the LHC. In Ref. [33], ATLAS carried out a search for the decay $H^\pm \to \tau\nu$ using the data taken with 8 TeV of collision energy and 19.5 fb^{-1} of integrated luminosity. From the non-observation of an excess above the SM prediction, the 95% CL lower limit on BR($t \to H^\pm b$) $\times$ BR($H^\pm \to \tau^\pm\nu$) has been given to be between 0.23% and 1.3% in the range 80 GeV $< m_{H^\pm} < 160$ GeV. Similar limits are derived in the CMS search in [34]. The search for $H^\pm$ with decay into cs has also been performed in [35] by CMS using 8 TeV data and 19.7 fb^{-1} of integrated luminosity. The 95% CL lower limit on BR($t \to H^\pm b$) $\times$ BR($H^\pm \to cs$) has been given to be between 1.2% and 6.5% in the range 90 GeV $< m_{H^\pm} < 160$ GeV. Similar

16

constraints are obtained from the ATLAS search for $H^\pm \to cs$ in [36]. We note that there is a local excess of 2.4σ around $m_{H^\pm} = 150$ GeV in the CMS search in [35], with a best-fit branching fraction of $t \to H^\pm b = 1.2 \pm 0.2\%$, assuming $\mathrm{BR}(H^\pm \to cs) = 100\%$.

In order to estimate the bound from these LHC direct searches in our 3HDMs, we require the following conditions as the strongest bound of which meaning is explained below:

$$\sum_{a=1,2} \mathrm{BR}(t \to H_a^\pm b) \times \mathrm{BR}(H_a^\pm \to \tau^\pm \nu) < 0.23\%, \tag{31}$$

$$\sum_{a=1,2} \mathrm{BR}(t \to H_a^\pm b) \times [\mathrm{BR}(H_a^\pm \to cs) + \mathrm{BR}(H_a^\pm \to cb)] < 1.2\%, \tag{32}$$

where these constraints can be applied to the case of $90\ \mathrm{GeV} < m_{H_{1,2}^\pm} < 160\ \mathrm{GeV}$. Regarding the second equation, we include the cb mode because no flavour tagging was employed in Ref. [35], see also [22, 37]. We note that the two charged Higgs boson contributions should not be summed if the mass difference between $H_1^\pm$ and $H_2^\pm$ is taken to be larger than the detector resolution. If we do not sum these two contributions, then we should get a milder bound than that obtained from Eqs. (31) and (32). Thus, the meaning of "strongest bound" is choosing the strongest limit on the product of two branching fractions (the top decay and the charged Higgs boson decay) in the given mass range and summing two charged Higgs boson contributions.

In Fig. 6, we show the allowed parameter space on the $m_{H_1^\pm}$-$m_{H_2^\pm}$ plane in the Type-Y 3HDM with $\tan\beta = 2$ and $\theta_C = -\pi/4$. The green shaded region is allowed from $B \to X_s \gamma$ data and the right region from the purple and the black curve satisfies the requirement given in Eqs. (31) and (32), respectively. The value of $\tan\gamma$ is taken to be 3, 5, 10, 15, 20 and 30 as indicated in each panel of the figure. We note that the region below the dashed curve, $m_{H_1^\pm} > m_{H_2^\pm}$, is excluded by definition. It is seen that the constraint from $H_{1,2}^\pm \to q\bar{q}'$ becomes stronger as compared to that from $H_{1,2}^\pm \to \tau\nu$ when we take a larger value of $\tan\gamma$, because of the enhancement of $\mathrm{BR}(H_{1,2}^\pm \to cb/cs)$, as we already saw in Fig. 1. Consequently, the case with $m_{H_1^\pm} < m_t - m_b$ and $m_{H_2^\pm} < m_t - m_b$ is highly constrained from $B \to X_s\gamma$ and the direct search at the LHC. However, we can find allowed regions with $m_{H_1^\pm} < m_t - m_b$ and $m_{H_2^\pm} > m_t - m_b$ and also those with $m_{H_1^\pm} > m_t - m_b$ and $m_{H_2^\pm} > m_t - m_b$. The former case is phenomenologically very interesting, because the lighter charged Higgs boson $H_1^\pm$ can mainly decay into the cb final state. The BR of the $H_1^\pm \to cb$ mode is shown in the caption of Fig. 6, and is essentially determined only by the value of $\tan\gamma$ for a fixed value of $\tan\beta$

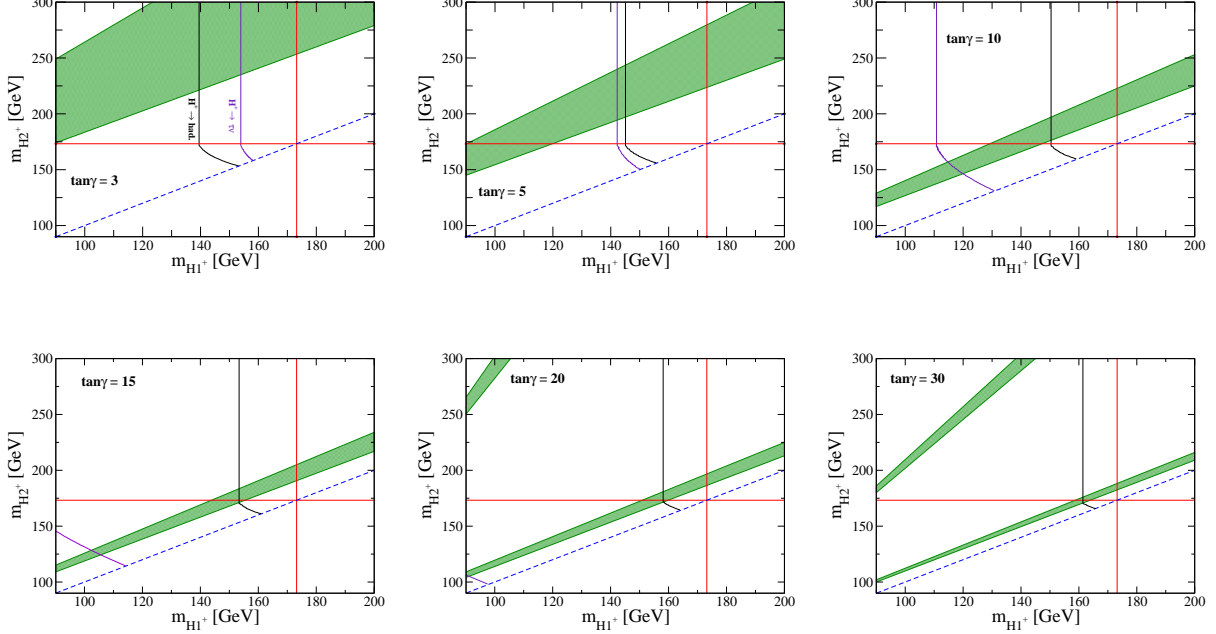FIG. 6: Green shaded regions indicate the 2σ allowed region by the $B \to X_s\gamma$ data in the Type-Y 3HDM with $\tan\beta = 2$ and $\theta_C = -\pi/4$. The value of $\tan\gamma$ is taken to be 3, 5, 10, 15, 20 and 30 from the upper left to lower right panel. The right region from the black and purple curve is allowed by the bound from the $t \to H_{1,2}^{\pm}b \to q\bar{q}'b$ (cs and cb) and $t \to H_{1,2}^{\pm}b \to \tau\nu b$ processes at the LHC. The branching ratio of $H_1^{\pm} \to cb$ is about 43%, 68%, 82%, 84%, 85% and 86% for the case with $\tan\gamma = 3$, 5, 10, 15, 20 and 30, respectively, and $m_{H_1^{\pm}} < m_t$.

and θ_C when $m_{H_1^{\pm}} < m_t$.

In Fig. 7, we also show a similar plot for the Type-Z 3HDM, where the constraint from $B \to X_s\gamma$ is exactly the same as that in the Type-Y 3HDM because of the same structure of the quark Yukawa couplings. The difference can be seen in the relative strength of the constraint from Eqs. (31) and (32) as compared to the Type-Y case. In analogy with the Type-Y case, the scenario with both charged Higgs boson masses smaller than $m_t - m_b$ is highly constrained by $B \to X_s\gamma$ and LHC direct searches, but at least one of the charged Higgs bosons can be lighter than the top quark. Similarly to Fig. 6, we give the value of the BR of $H_1^{\pm} \to cb$ in the caption of this figure.

It is particularly interesting to investigate the case with a charged Higgs boson mass between 80 GeV and 90 GeV, and $H^{\pm}$ decaying dominantly to cs/cb. In this situation, the bound from direct searches at the LHC cannot be applied to exclude any parameter
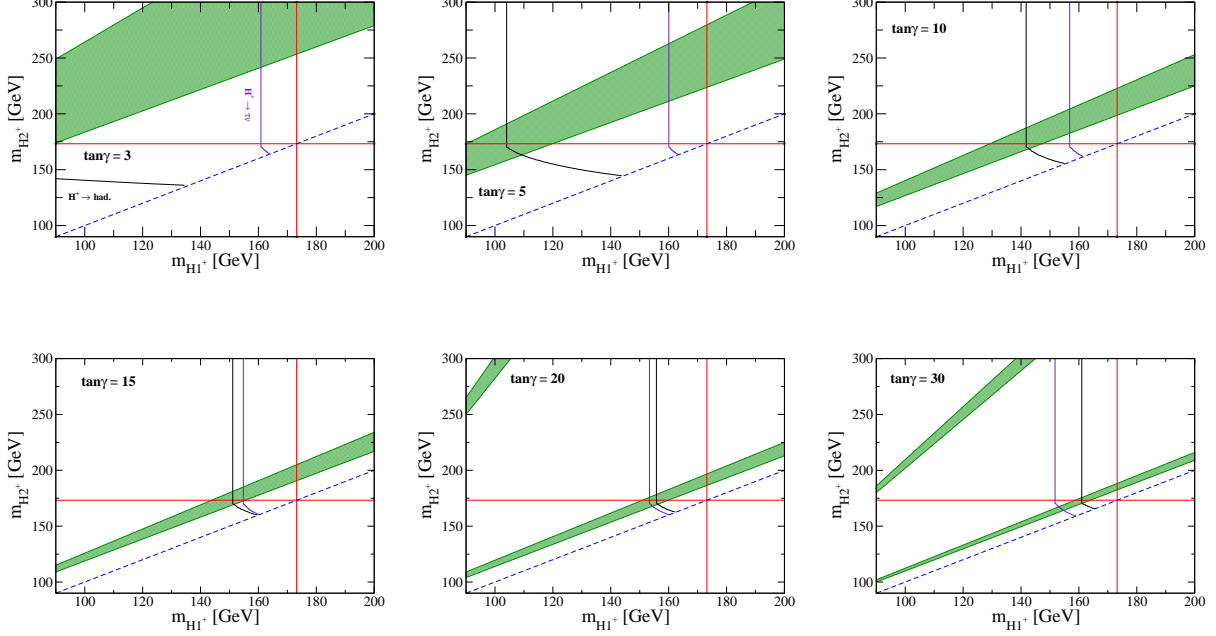
FIG. 7: Same as Fig. 6, but for the case of Type-Z 3HDM. The branching ratio of $H_1^\pm \to cb$ is about 4%, 16%, 50%, 67%, 75% and 81% for the case with $\tan\gamma = 3, 5, 10, 15, 20$ and 30, respectively, and $m_{H_1^\pm} < m_t$.

space because no sensitivity exists in this mass region. This is because the background from $t \to W^\pm b$ is overwhelming in this region and the invariant mass cut on the jets originating from $H^\pm$ would lose its effect of greatly suppressing the background when $m_{H^\pm}$ is close to m_W. However, searches for $H^\pm$ from LEP2 and the Tevatron have some sensitivity to this region of charged Higgs boson mass between 80 GeV and 90 GeV and we include these bounds in our analysis. In Ref. [38], the excluded region in the $m_{H^\pm}$-BR($H^\pm \to \tau\nu$) plane has been given by using the combined LEP2 data from all four experiments. If we take $m_{H_1^\pm} = 83$ GeV, we can extract the bound BR($H_1^\pm \to \tau\nu$) $\lesssim 0.45$ at the 95% CL, with the exact bound depending on the choice of $m_{H_1^\pm}$ i.e. there is a sizeable region of unexcluded parameter space where BR($H_1^\pm \to cs/cb$) is sizeable and $80\,\text{GeV} < m_{H_1^\pm} < 90$ GeV. We note that the results of the LEP2 search in Ref. [38] show that there are some regions of BR($H_1^\pm \to cs/cb$) and $80\,\text{GeV} < m_{H_1^\pm} < 90$ GeV where there are fluctuations in excess of 2σ above the background. In Ref. [39], we can also extract the bound BR($t \to H^+b$) $\times$ BR($H_1^\pm \to q\bar{q}'$) $\lesssim 0.2$ at the 95% CL from the data collected at the Tevatron with 1.0 fb^{-1}. The reason why this Tevatron search has sensitivity to charged Higgs masses between 80 GeV and 90 GeV is because no
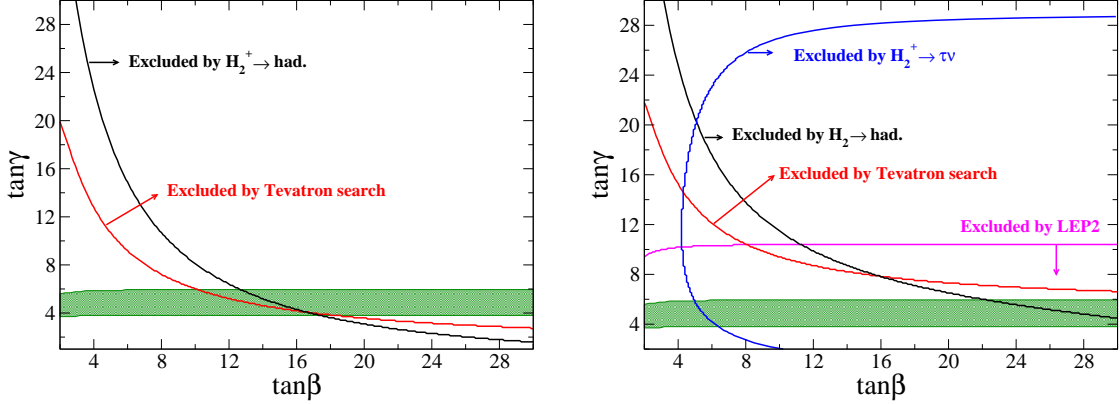
FIG. 8: Allowed parameter space by several constraints on the $\tan\beta$-$\tan\gamma$ plane in the Type-Y (left) and Type-Z (right) 3HDM with $m_{H_1} = 83$ GeV, $m_{H_2^\pm} = 160$ GeV and $\theta_C = -\pi/4$. The right region from the blue, black and red curve is excluded by Eq. (31), Eq. (32) and the Tevatron data, respectively. The region below the magenta curve is also excluded by the LEP2 data. The green shaded region is allowed by the measurement of $B \to X_s\gamma$.

invariant mass cut is used, and instead a disappearance search is carried out. So far the LHC searches have not used this search strategy.

By imposing these two constraints (from LEP2 and Tevatron) for $H_1^\pm$ and those from Eqs. (31) and (32) for $H_2^\pm$, we obtain the excluded region on the $\tan\beta$-$\tan\gamma$ plane shown in Fig. 8. In this figure, we take $m_{H_1^\pm} = 83$ GeV, $m_{H_2^\pm} = 160$ GeV and $\theta_C = -\pi/4$. The left and right panel show the case in the Type-Y and Type-Z 3HDM, respectively. The green shaded region is allowed by the $B \to X_s\gamma$ data. As we can see, in the Type-Z 3HDM, there is no region satisfying all the constraints mentioned above. In contrast, we can find allowed regions in the Type-Y case, namely, when $4 \lesssim \tan\gamma \lesssim 6$ and $\tan\beta < 10$-18.

IV. PHENOMENOLOGY OF 3HDM CHARGED HIGGS BOSONS AT THE LHC

The collider phenomenology of a charged Higgs boson can be classified into two regimes depending on its mass $m_{H^\pm}$: (i) $m_{H^\pm} < m_t - m_b$ (light) and (ii) $m_{H^\pm} > m_t - m_b$ (heavy). For case (i), charged Higgs bosons can be produced via the top quark decay, so that the main production process at the LHC is $gg, q\bar{q} \to t\bar{t} \to H^+ b\bar{t}$ (see Fig. 9). For case (ii), the main production mode is the top quark associated process, i.e., $gb \to H^\pm t$ + c.c. As

	$(m_{H_1^\pm}, m_{H_2^\pm}, \tan\gamma)$	$\mathrm{BR}(H_1^\pm \to X)_\mathrm{Y}$	$\mathrm{BR}(H_2^\pm \to X)_\mathrm{Y}$	$\mathrm{BR}(H_1^\pm \to X)_\mathrm{Z}$	$\mathrm{BR}(H_2^\pm \to X)_\mathrm{Z}$
BM1:	$(83, 160, 5)$	$cb : 68, cs : 17$	$cb : 77, cb : 16$	-	-
BM2:	$(160, 250, 3)$	$cb : 43, \tau\nu : 34$	$tb : 99.7, cb : 0.17$	$\tau\nu : 94, cb : 4.0$	$tb : 99.7, ts : 0.17$
BM3:	$(160, 225, 5)$	$cb : 68, cs : 17$	$tb : 99.6, cb : 0.21$	$\tau\nu : 80, cb : 16$	$tb : 99.4, cb : 0.21$
BM4:	$(160, 200, 10)$	$cb : 82, cs : 15$	$tb : 98, cb : 1.3$	$cb : 50, \tau\nu : 41$	$tb : 98, cb : 1.3$
BM5:	$(160, 180, 20)$	$cb : 85, cs : 14$	$tb : 67, cb : 28$	$cb : 75, \tau\nu : 13$	$tb : 66, cb : 27$
BM6:	$(200, 250, 10)$	$tb : 99.0, cb : 0.89$	$tb : 99.5, cb : 0.29$	$tb : 98, cb : 0.89$	$tb : 99.4, cb : 0.29$

TABLE III: Predictions of the biggest two values of $\mathrm{BR}(H_{1,2}^\pm \to X)$ in the Type-Y and Type-Z 3HDM for the six benchmark points (BM1-BM6) which are allowed by $B \to X_s\gamma$ and direct searches at LEP2, Tevatron and LHC. We take $\tan\beta = 2$ and $\theta_C = -\pi/4$. The values of $m_{H_1^\pm}$ and $m_{H_2^\pm}$ are presented in GeV while those for the BRs are in %. For BM1, only the Type-Y is allowed, so that we do not show the predictions in the Type-Z 3HDM.
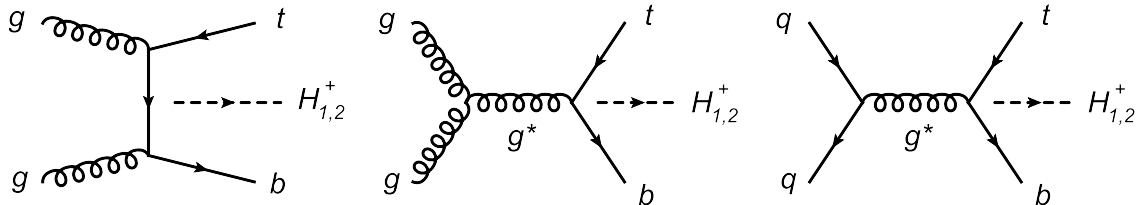

FIG. 9: Topologies of the Feynman diagram for the $gg \to \bar{t}bH_{1,2}^+$ (left and middle) and $q\bar{q} \to \bar{t}bH_{1,2}^+$ (right) processes. The charged Higgs bosons can be emitted from the final state quark current at 3 (left) and 2 (middle and right) different points. For the topology on the left, gluon permutations are also required. In total, one has 8(2) diagrams for the $gg(q\bar{q})$-induced process (at fixed q flavour).

intimated, See Fig. 9, we will use the $gg \to t\bar{b}H^- + $ c.c. subprocess (at LO) in our Monte Carlo (MC) analysis, which captures both (i) (limited to the gg channel) and (ii) as well as their interference, which is important in the threshold region $m_{H^\pm} \sim m_t - m_b$ [40, 41]. (In fact, we will also be emulating the subleading contribution from $q\bar{q} \to t\bar{b}H^- + $ c.c.) Recall that, on the one hand, in the narrow width approximation of the top quark one has that $\sigma(gg, q\bar{q} \to t\bar{b}H^-) \equiv \sigma(gg, q\bar{q} \to t\bar{t}) \times \mathrm{BR}(\bar{t} \to \bar{b}H^-)$ (limited to the diagrams in which the H^- is emitted by the t antiquark) and, on the other hand, the b-quark in the initial state

21

comes from a gluon splitting inside the proton, as explained in [40, 41].

In order to encourage phenomenological studies for the charged Higgs bosons at the LHC, we present six benchmark parameter sets, BM1–BM6, allowed by the $B \rightarrow X_s\gamma$ data and direct searches at LEP2, Tevatron and LHC in Tab. III. Herein, the biggest two values of BRs for $H_1^\pm$ and $H_2^\pm$ are given in the Type-Y and Type-Z 3HDM for each of the six benchmark points. We will particularly use BM1, BM4 and BM6 in the Type-Y case for our forthcoming MC analysis, as illustrative of the three situations emerged so far: of a light, mixed and heavy charged Higgs mass spectrum, respectively, with respect to the top quark mass. While we refer to the Type-Y 3HDM case in the remainder of our analysis, we confirm that the ensuing phenomenology is not dissimilar in the Type-Z 3HDM case (except for BM1 which is not allowed herein).

For the MC study we have computed the following signal (S) and (irreducible) background (B) processes, respectively:

$$\text{a. } gg, q\bar{q} \rightarrow t\bar{b}H_{1,2}^- + \text{c.c} \rightarrow t\bar{b}jj + \text{c.c,}$$

$$\text{b. } gg, q\bar{q} \rightarrow t\bar{b}W^- + \text{c.c.} \rightarrow t\bar{b}jj + \text{c.c.,}$$

where the di-jet system jj is tagged through a single b-tag, as recommended in [22]. We remind the reader here that applying such a b-tag would improve sensitivity to $H_{1,2}^\pm \rightarrow cb$ decays greatly, as the background from $W \rightarrow cb$ has a very small rate. This is made explicit by choosing a b-tagging efficiency $\epsilon_b = 0.5$, a c-quark mistagging rate $\epsilon_c = 0.1$ and a light quark (u, d, s) mistagging rate $\epsilon_j = 0.01$. It follows that the estimate gain in sensitivity with respect to the case in which the di-jet system is untagged is then:

$$\frac{[S/\sqrt{B}]_{\text{btag}}}{[S/\sqrt{B}]_{\not{b}\text{tag}}} \sim \frac{\epsilon_b\sqrt{2}}{\sqrt{(\epsilon_j + \epsilon_c)}} \sim 2.13. \tag{33}$$

Fig. 10 shows the di-jet mass distribution for S and B at 13 TeV in terms of cross section for BM1, BM4 and BM6. Even before enforcing any selection cuts, it is clear the LHC potential in accessing these peculiar 3HDM signatures during Run 2. Two caveats should be borne in mind here though. On the one hand, we have not allowed for full combinatorial effects in the di-jet mass reconstruction, as we have assumed that each of the three b-jets present in the final state can be correctly assigned to its parent heavy particle (i.e., t, $\bar{t}$ and $H_{1,2}^\pm$). On the other hand, BM1, BM4 and BM6 are the very best points for our purposes, those with highest BR, while one really ought to test the entire parameter space of 3HDMs
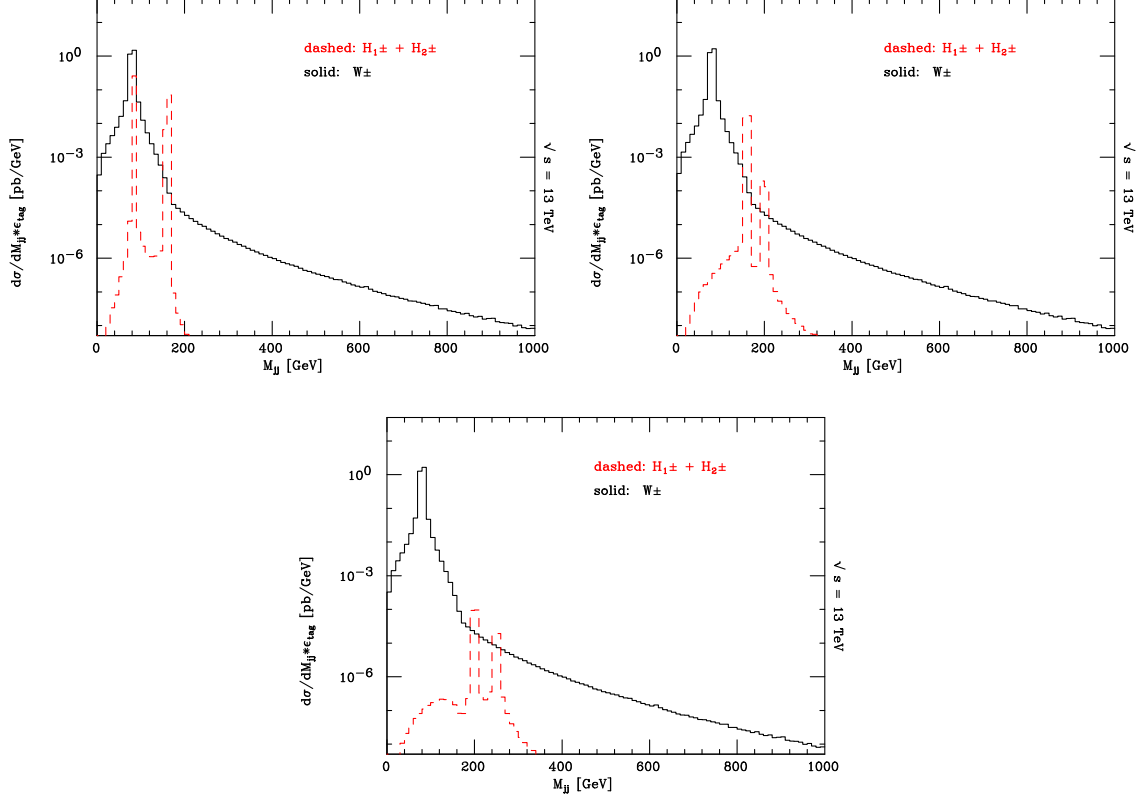
FIG. 10: Differential distributions in the di-jet invariant mass of processes a (red dashed) and b (black solid) for the BM1 (top-left), BM4 (top-right) and BM6 (bottom) at the LHC with $\sqrt{s} = 13$ TeV. Tagging efficiencies are included as described in the text. CTEQ(4L) with $Q = \mu = \sqrt{\hat{s}}$ is used [42].

sampled over the inputs θ_C, $\tan\beta$, $\tan\gamma$, $m_{H_1^\pm}$ and $m_{H_2^\pm}$. Nonetheless, we believe that the very peculiar $H_{1,2}^\pm$ mass patterns that we have discussed deserve further investigation in presence of parton shower, hadronisation, jet reconstruction and detector effects [43].

Finally, we briefly comment on the phenomenology of the additional neutral Higgs bosons $H_{1,2}$ and $A_{1,2}$ in the 3HDMs. When we consider the case with the masses of $H_{1,2}^\pm$ to be $\mathcal{O}(100)$ GeV, the neutral Higgs bosons cannot be so heavy due to the constraints from electroweak precision observables such as the S and T parameters [44] and from perturbative unitarity [30]. If we consider the case where these neutral Higgs bosons are heavier than the charged Higgs bosons, then there are no additional decay modes of the charged Higgs bosons beyond those shown in this paper. However, in this case, the decay channels $H_{1,2}/A_{1,2} \to H_{1,2}^\pm W^{(*)\mp}$ can be dominant depending on the mass difference between the neu-

tral Higgs states and the charged Higgs states, and the numerical values of the X_a, Y_a and Z_a parameters defined in Eqs. (17)-(19). These cascade decay channels would be additional production modes of $H_{1,2}^\pm$ beyond those studied in this section, although they would require a separate signal-background study in order to assess the detection prospects.

V.   CONCLUSIONS

We have discussed the phenomenology of charged Higgs bosons in fully active 3HDMs with two softly-broken discrete Z_2 symmetries which are imposed to avoid FCNCs at tree level. Under these Z_2 symmetries, we have defined five types of Yukawa interactions. We have then shown that the decay branching fractions of $H_{1,2}^\pm \to cb$ can be dominant in the Type-Y and Type-Z 3HDM when the masses of the charged Higgs bosons are taken to be below $m_t - m_b$. The $H^\pm \to cb$ decay can also be dominant in the Type-Y 2HDM with $m_{H^\pm} < m_t - m_b$, but such a light charged Higgs boson scenario is excluded by the constraint from $B \to X_s\gamma$. In contrast, in 3HDMs, the scenario with masses of $\mathcal{O}(100)$ GeV for the charged Higgs bosons is allowed by $B \to X_s\gamma$ because of a cancellation between the separate contributions from the $H_1^\pm$ and $H_2^\pm$ loop diagrams. Therefore, the search for a light charged Higgs boson decaying into cb is a means to distinguish 3HDMs from 2HDMs.

We then have calculated the branching fraction of the $B \to X_s\gamma$ process at NLO in QCD in 3HDMs in order to confirm how the cancellation takes place numerically. We found that it happens especially in the Type-II, Type-Y and Type-Z 3HDMs when there is a non-zero mixing and a mass difference between $H_1^\pm$ and $H_2^\pm$. In the Type-I and Type-X 3HDMs, the numerical values of BR$(B \to X_s\gamma)$ are not much different from the predictions in Type-I and Type-X 2HDMs.

We also have taken into account the constraints from direct searches at the LHC of charged Higgs bosons from the top quark decays $t \to H^\pm b \to \tau\nu b$ and $t \to H^\pm b \to q\bar{q}'b$ with the 8 TeV data. We have found that, in the Type-Y and Type-Z 3HDM, the scenario with both $H_1^\pm$ and $H_2^\pm$ lighter than $m_t - m_b$ is highly constrained from $B \to X_s\gamma$ and the LHC direct searches, while the scenario with only $H_1^\pm$ lighter than $m_t - m_b$ is allowed. However, the particular case $m_{H_1^\pm} \approx m_{W^\pm}$ with $m_{H_2^\pm} < m_t$ is allowed (also by Tevatron and LEP2), albeit only in the Type-Y 3HDM. We drew attention to the fact that the region of $80\,\mathrm{GeV} < m_{H_1^\pm} < 90$ GeV is not constrained by current LHC searches for $t \to H^\pm b$ followed

by dominant decay $H^\pm \to cs/cb$, and this parameter space is only weakly constrained from LEP2 and Tevatron searches. Any future signal in this region could be readily accommodated by $H_1^\pm$ from a 3HDM

Finally, upon running a MC simulation to compare the yield of the $H_{1,2}^\pm$ signals and $W^\pm$ background through the production processes $gg, q\bar{q} \to t\bar{b}H_{1,2}^- + \text{c.c}$ and $gg, q\bar{q} \to t\bar{b}W^- + \text{c.c}$, respectively, followed by the corresponding di-jet decays $H_{1,2}^\pm \to jj$ and $W^\pm \to jj$, we have shown that the aforementioned charged Higgs boson signals should be accessible at Run 2 of the LHC over a suitable region of the 3HDM parameter space, provided that b-tagging is enforced so as to single out the cb component above the cs one. Therefore, these (multiple) charged Higgs boson signatures can be used not only to distinguish between 2HDMs and 3HDMs but also to identify the types realising the latter.

Acknowledgements

Note added:

After this work was completed an explicit search for $t \to H^+ b$ followed by the decay $H^+ \to cb$ was carried out by the CMS collaboration in CMS PAS HIG-16-030, with 19.7 fb^{-1} of data at $\sqrt{s} = 8$ TeV. Stronger upper limits on the branching ratio of $t \to H^+ b$ have been probed than for the CMS search for $t \to H^+ b$, $H^+ \to cs$ in Ref. [35] with the same data sample. This result explicitly shows the increase in sensitivity that can be obtained by tagging a third b quark.

Appendix A: Mass matrix elements

We present here the analytic expressions for the mass matrices of the singly-charged ($\mathcal{M}_C^2$), CP-odd ($\mathcal{M}_A^2$) and CP-even ($\mathcal{M}_H^2$) scalar states in the Higgs basis of 3HDMs. The matrix elements of $\mathcal{M}_C^2$ and $\mathcal{M}_A^2$ are given by

$$(\mathcal{M}_C^2)_{11} = -\frac{v^2}{2}\left[(\rho_2 + \rho_3)c_\gamma^2 + (\kappa_2 + \kappa_3)s_\gamma^2\right] + \mu_{12}^2\frac{c_\gamma}{s_\beta c_\beta} + \mu_{23}^2\frac{s_\gamma}{s_\beta c_\beta}, \tag{A1}$$

$$\begin{aligned}(\mathcal{M}_C^2)_{22} = &-\frac{v^2}{2}\left[(\rho_2 + \rho_3)s_\beta^2 s_\gamma^2 + (\sigma_2 + \sigma_3)c_\beta^2 + (\kappa_2 + \kappa_3)s_\beta^2 c_\gamma^2\right] \\ &+ \mu_{12}^2 t_\beta s_\gamma t_\gamma + \frac{\mu_{13}^2}{s_\gamma c_\gamma} + \mu_{23}^2\frac{t_\beta c_\gamma}{t_\gamma},\end{aligned} \tag{A2}$$

$$(\mathcal{M}_C^2)_{12} = -\frac{v^2}{4}(\rho_2 + \rho_3 - \kappa_2 - \kappa_3)s_\beta s_{2\gamma} + \mu_{12}^2\frac{s_\gamma}{c_\beta} - \mu_{23}^2\frac{c_\gamma}{c_\beta}, \tag{A3}$$

$$(\mathcal{M}_A^2)_{11} = -v^2\left(\rho_3 c_\gamma^2 + \kappa_3 s_\gamma^2\right) + \mu_{13}^2\frac{c_\gamma}{s_\beta c_\beta} + \mu_{23}^2\frac{s_\gamma}{s_\beta c_\beta}, \tag{A4}$$

$$(\mathcal{M}_A^2)_{22} = -v^2\left(\rho_3 s_\beta^2 s_\gamma^2 + \sigma_3 c_\beta^2 + \kappa_3 s_\beta^2 c_\gamma^2\right) + \mu_{12}^2 t_\beta s_\gamma t_\gamma + \mu_{13}^2\frac{s_\gamma}{s_\gamma c_\gamma} + \mu_{23}^2\frac{t_\beta c_\gamma}{t_\gamma}, \tag{A5}$$

$$(\mathcal{M}_A^2)_{12} = -\frac{v^2}{2}(\rho_3 - \kappa_3)s_\beta s_{2\gamma} + \mu_{12}^2\frac{s_\gamma}{c_\beta} - \mu_{23}^2\frac{c_\gamma}{c_\beta}. \tag{A6}$$

Those for $\mathcal{M}_H^2$ are given by

$$(\mathcal{M}_H^2)_{11} = \frac{v^2}{2}(2\lambda_1 c_\beta^4 c_\gamma^4 + 2\lambda_2 s_\beta^4 + 2\lambda_3 c_\beta^4 s_\gamma^4 + \rho_{123} s_{2\beta}^2 c_\gamma^2 + \sigma_{123} c_\beta^4 s_{2\gamma}^2 + \kappa_{123} s_{2\beta}^2 s_\gamma^2), \tag{A7}$$

$$\begin{aligned}(\mathcal{M}_H^2)_{22} = &\frac{v^2}{8}(2\lambda_1 s_{2\beta}^2 c_\gamma^4 + 2\lambda_2 s_{2\beta}^2 + 2\lambda_3 s_{2\beta}^2 s_\gamma^4 - 4\rho_{123} c_\beta^2 s_{2\gamma}^2 + \sigma_{123} s_{2\beta}^2 s_{2\gamma}^2 - 4\kappa_{123} s_{2\beta}^2 s_\gamma^2) \\ &+ \mu_{12}^2\frac{c_\gamma}{s_\beta c_\beta} + \mu_{23}^2\frac{s_\gamma}{s_\beta c_\beta},\end{aligned} \tag{A8}$$

$$(\mathcal{M}_H^2)_{33} = \frac{v^2}{4}(\lambda_1 + \lambda_3 - 2\sigma_{123})c_\beta^2 s_{2\gamma}^2 + \mu_{12}^2 t_\beta s_\gamma t_\gamma + \frac{\mu_{13}^2}{s_\gamma c_\gamma} + \mu_{23}^2\frac{c_\gamma t_\beta}{t_\gamma}, \tag{A9}$$

$$\begin{aligned}(\mathcal{M}_H^2)_{12} = &-\frac{v^2}{2}\Big[2\lambda_1 s_\beta c_\beta^3 c_\gamma^4 - 2\lambda_2 s_\beta^3 c_\beta + 2\lambda_3 s_\beta c_\beta^3 s_\gamma^4 \\ &- (c_\beta + c_{3\beta})s_\beta c_\gamma^2\rho_{123} + s_\beta c_\beta^3 s_{2\gamma}^2\sigma_{123} - (c_\beta + c_{3\beta})s_\beta s_\gamma^2\kappa_{123}\Big],\end{aligned} \tag{A10}$$

$$(\mathcal{M}_H^2)_{13} = -\frac{v^2}{4}\left(2\lambda_1 c_\beta^3 s_{2\gamma}c_\gamma^2 - 2\lambda_3 c_\beta^3 s_{2\gamma}s_\gamma^2 + 2\rho_{123}s_\beta^2 c_\beta s_{2\gamma} - \sigma_{123}c_\beta^3 s_{4\gamma} - 2\kappa_{123}s_\beta^2 c_\beta s_{2\gamma}\right), \tag{A11}$$

$$(\mathcal{M}_H^2)_{23} = \frac{v^2}{4}[4\lambda_1 s_\gamma c_\gamma^3 - 4\lambda_3 s_\gamma^3 c_\gamma - 2(\rho_{123} - \kappa_{123})s_{2\gamma} - \sigma_{123}s_{4\gamma}]s_\beta c_\beta^2 + \mu_{12}^2\frac{s_\gamma}{c_\beta} - \mu_{23}^2\frac{c_\gamma}{c_\beta}. \tag{A12}$$

In the above expressions, we used the shorthand notations $c_X = \cos X$, $s_X = \sin X$ and $t_X = \tan X$.

Appendix B: Input parameters

For the numerical evaluations, we have used the following input values for the SM parameters [45]:

$$m_{W^\pm} = 80.385 \text{ GeV}, \ m_Z = 91.1876 \text{ GeV}, \ G_F = 1.1663787 \times 10^{-5} \text{ GeV}^{-2},$$

$$m_\tau = 1.77684 \text{ GeV}, \ m_\mu = 0.105658367 \text{ GeV},$$

$$\alpha_s(m_Z) = 0.1185, \ m_t^{\text{pole}} = 174.6 \text{ GeV}, \ m_b^{\text{pole}} = 4.89 \text{ GeV}, \ m_c^{\text{pole}} = 1.64 \text{ GeV}, \qquad \text{(B1)}$$

where m_t^{pole}, m_b^{pole} and m_c^{pole} are respectively the pole masses of the top, bottom and charm quark. For the $\overline{\text{MS}}$ masses of the quarks, we use the following values [45]:

$$\bar{m}_b(\bar{m}_b) = 4.18 \text{ GeV}, \ \bar{m}_c(\bar{m}_c) = 1.275 \text{ GeV}, \ \bar{m}_s(2 \text{ GeV}) = 0.0935 \text{ GeV}. \qquad \text{(B2)}$$

Using these $\overline{\text{MS}}$ masses, we obtain the running masses of the quarks at, e.g., $\mu = 100$ GeV to be $\bar{m}_b = 3.01$ GeV, $\bar{m}_c = 0.701$ GeV and $\bar{m}_s = 0.0489$ GeV. As for the other inputs, we use

$$|V_{tb}V_{ts}/V_{cb}|^2 = 0.9626, \ \text{BR}(B \to X_c \ell \nu) = 0.1065. \qquad \text{(B3)}$$

for the calculation of $\text{BR}(B \to X_s \gamma)$ and

$$|V_{cb}| = 0.0409 \qquad \text{(B4)}$$

for that of the charged Higgs boson decays.

[1] G. Aad *et al.* [ATLAS Collaboration], Phys. Lett. B **716**, 1 (2012).

[2] S. Chatrchyan *et al.* [CMS Collaboration], Phys. Lett. B **716**, 30 (2012).

[3] H. E. Haber and G. L. Kane, Phys. Rept. **117**, 75 (1985).

[4] N. Turok and J. Zadrozny, Phys. Rev. Lett. **65**, 2331 (1990).

[5] A. I. Bochkarev, S. V. Kuzmin and M. E. Shaposhnikov, Phys. Rev. D **43**, 369 (1991).

[6] A. E. Nelson, D. B. Kaplan and A. G. Cohen, Nucl. Phys. B **373**, 453 (1992).

[7] A. Zee, Phys. Lett. B **93**, 389 (1980) [Erratum-ibid. B **95**, 461 (1980)] and Phys. Lett. B **161**, 141 (1985).

[8] R. Barbieri, L. J. Hall and V. S. Rychkov, Phys. Rev. D **74**, 015007 (2006).

[9] M. Ciuchini, E. Franco, G. Martinelli, L. Reina and L. Silvestrini, Phys. Lett. B **334**, 137 (1994).

[10] M. Ciuchini, G. Degrassi, P. Gambino and G. F. Giudice, Nucl. Phys. B **527**, 21 (1998).

[11] F. Borzumati and C. Greub, Phys. Rev. D **58**, 074004 (1998).

[12] P. Gambino and M. Misiak, Nucl. Phys. B **611**, 338 (2001).

[13] T. Hermann, M. Misiak and M. Steinhauser, JHEP **1211**, 036 (2012).

[14] M. Misiak, H. M. Asatrian, R. Boughezal, M. Czakon, T. Ewerth, A. Ferroglia, P. Fiedler and P. Gambino *et al.*, Phys. Rev. Lett. **114**, 221801 (2015).

[15] V. D. Barger, J. L. Hewett and R. J. N. Phillips, Phys. Rev. D **41**, 3421 (1990).

[16] Y. Grossman, Nucl. Phys. B **426**, 355 (1994).

[17] A. G. Akeroyd, Phys. Lett. B **377**, 95 (1996).

[18] M. Aoki, S. Kanemura, K. Tsumura and K. Yagyu, Phys. Rev. D **80**, 015017 (2009).

[19] A. G. Akeroyd and W. J. Stirling, Nucl. Phys. B **447**, 3 (1995).

[20] A. G. Akeroyd, hep-ph/9509203.

[21] G. Cree and H. E. Logan, Phys. Rev. D **84**, 055021 (2011).

[22] A. G. Akeroyd, S. Moretti and J. Hernandez-Sanchez, Phys. Rev. D **85**, 115002 (2012).

[23] A. G. Akeroyd, Nucl. Phys. B **544**, 557 (1999).

[24] D. J. Miller, S. Moretti, D. P. Roy and W. J. Stirling, Phys. Rev. D **61**, 055011 (2000).

[25] O. Eberhardt, U. Nierste and M. Wiebusch, JHEP **1307**, 118 (2013).

[26] I. P. Ivanov, JHEP **1007**, 020 (2010).

[27] I. P. Ivanov and E. Vdovin, Phys. Rev. D **86**, 095030 (2012).

[28] V. Keus, S. F. King and S. Moretti, JHEP **1401**, 052 (2014).

[29] M. Maniatis and O. Nachtmann, JHEP **1502**, 058 (2015) Erratum: [JHEP **1510**, 149 (2015)].

[30] S. Moretti and K. Yagyu, Phys. Rev. D **91**, 055022 (2015).

[31] J. L. Hewett, in 'Stanford 1993, Proceedings, Spin structure in high energy processes', 463-475, and hep-ph/9406302.

[32] Y. Amhis *et al.* [Heavy Flavor Averaging Group (HFAG) Collaboration], arXiv:1412.7515 [hep-ex].

[33] G. Aad *et al.* [ATLAS Collaboration], JHEP **1503**, 088 (2015).

[34] V. Khachatryan *et al.* [CMS Collaboration], JHEP **1511**, 018 (2015).

[35] V. Khachatryan *et al.* [CMS Collaboration], JHEP **1512**, 178 (2015).

[36] G. Aad *et al.* [ATLAS Collaboration], Eur. Phys. J. C **73**, no. 6, 2465 (2013).

[37] S. Moretti, A.G. Akeroyd and J. Hernandez-Sanchez, PoS Charged **2014**, 025 (2014).

[38] G. Abbiendi *et al.* [ALEPH and DELPHI and L3 and OPAL and LEP Collaborations], Eur. Phys. J. C **73**, 2463 (2013).

[39] V. M. Abazov *et al.* [D0 Collaboration], Phys. Lett. B **682**, 278 (2009).

[40] M. Guchait and S. Moretti, JHEP **0201**, 001 (2002).

[41] K. A. Assamagan, M. Guchait and S. Moretti, hep-ph/0402057.

[42] H. L. Lai, J. Huston, S. Kuhlmann, F. I. Olness, J. F. Owens, D. E. Soper, W. K. Tung and H. Weerts, Phys. Rev. D **55**, 1280 (1997).

[43] A. G. Akeroyd, S. Moretti, K. Yagyu and E. Yildirim, in preparation.

[44] A. E. Crcamo Hernndez, S. Kovalenko and I. Schmidt, Phys. Rev. D **91**, 095014 (2015).

[45] K. A. Olive *et al.* [Particle Data Group Collaboration], Chin. Phys. C **38**, 090001 (2014).